Multiple Views of Internal Tides and Mesoscales from Altimetric SSH, High Density XBTs, and the PIRATA Moorings

Edward D. Zaron (Portland State University)

Summary

• Agreement is found between XBT-derived dynamic height and Jason SSH in the Tropical Atlantic.

• Near the PIRATA mooring at 23°W the mesoscale spectrum of SSH is approximately k^{-1} at wavelengths shorter than 300km but it is not well-determined due to altimeter noise. At larger scales the SSH spectrum is approximately k^{-3}.

• There is tenuous evidence for an internal tide-related peak in the spectrum of SSH near 23°W.

• Acoustic Doppler Current Profiler (ADCP) data from the PIRATA mooring show clear evidence of tides.

• The tidal currents in the ADCP time series are non-stationary. Tide-band variance is not phase locked to the astronomical tidal forcing.

• The kinetic energy spectrum of the ADCP data is proportional to k^{-2} at periods longer than 12 hours, or at wavelengths longer than 30km if Taylor's frozen turbulence hypothesis is assumed.

• At periods shorter than 12 hours there is an apparent shift in energy level, but the slope of the spectrum is not well-determined due to measurement noise.

Introduction

The stationary and non-stationary components of the low-mode internal tide have recently been observed using data from the TOPEX/JASON-1/2 series of satellite altimeters. The non-stationary internal tide arises through interactions of the tide with non-tidal processes, and it has been hypothesized as a source of ambient internal wave energy in the ocean. The non-stationary internal tide is one route through which tides may contribute to mixing in the main thermocline and the maintenance of the global meridional overturning circulation, accurately quantifying energy in the non-stationary tide from altimetry is problematic, because of the relatively low signal-to-noise ratio of SSH variance within the mode-1 internal tide waveband.

In this poster we seek to systematically validate the altimteric SSH data, quantify the altimeter noise, investigate the non-tidal SSH spectrum, and compare with in situ current data. Work is ongoing to extend this analysis to sites in the Equatorial Pacific.

Comparison of Jason-1 SSH with Dynamic Height along High-Density Repeat Track XBT AX08
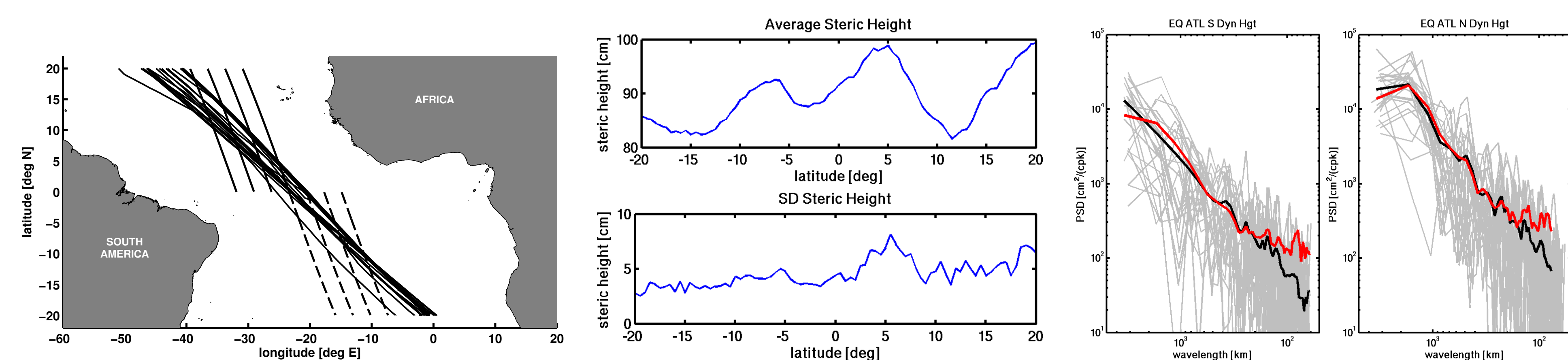
(a) AX08 XBT Transects and Jason-1 Ground Tracks. Note that transects are not aligned with Jason-1 ground tracks; hence, narrow band processes will appear at different wavelengths in wavenumber spectra.

(b) Mean (top) and standard deviation (bottom) dynamic height relative to 500m.

(c) Dynamic height spectra: gray – periodogram for each transect; black – average of conventional periodograms; red – average of Lombe-Scargle periodograms.

Figure 1: Analysis of AX08 dynamic height. The AX08 high-density repeat XBT transect has been occupied approximately 4 times per year since 2002; twenty five transects are used here. There is a difference in dynamic height variability between the northern and southern equatorial regions (middle, bottom); hence, power spectra a computed separately for the northern and southern hemisphere data. The nominal spacing of the XBTs is about 30km. The interpolation of these data to a regularly-spaced series for spectral analysis leads to a high-wavenumber artifact in the spectrum (right, black lines). When the Lombe-Scargle periodogram is used instead (right, red lines), the high-wavenumber behavior of the spectra is consistent with the error level of dynamic height.
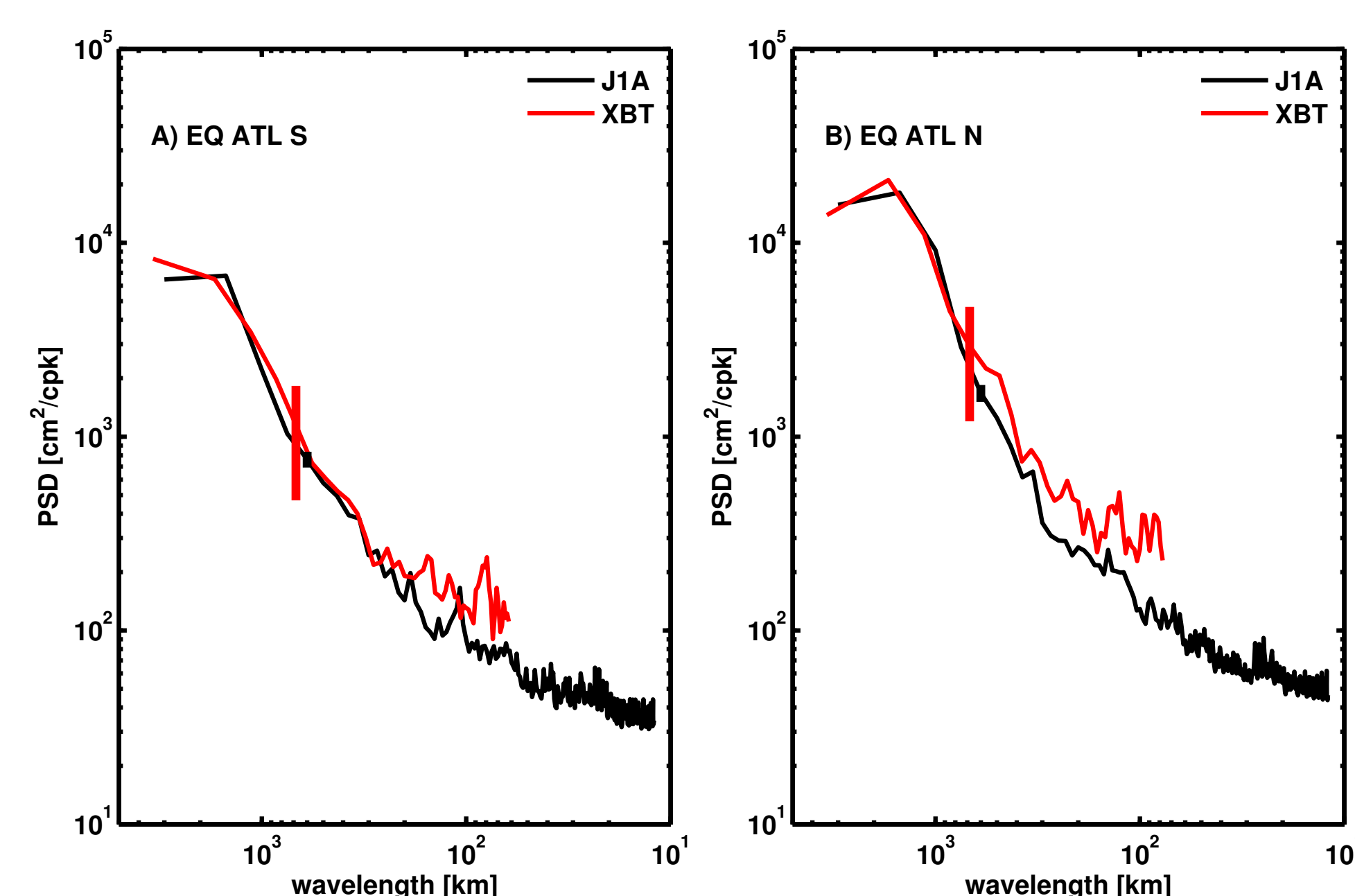
Figure 2: Jason-1 vs. XBT Power Spectra. Wavenumber power spectrum is shown for surface dynamic height relative to 500m derived from AX08 XBT transects (red) and Jason-1 SSH anomaly (black). Spectra are averaged over (A) −20°N to 0° latitude range, and (B) 0° to 20°N in (B). This vertical lines show the 99% confidence limits on the spectra. Jason-1 and AX0 dynamic height spectra agree well for scales larger than 200km. At shorter scales the XBT-derived dynamic height is inaccurate due to the inference of salinity from climatology.

Comparison of Jason-1 with TOPEX/POSEIDON During the Calibration Phase

(a) −20°N to Equator

(b) −10°N to 10° near 23°W

(c) −10°N to 10° near 23°W: COMPENSATED
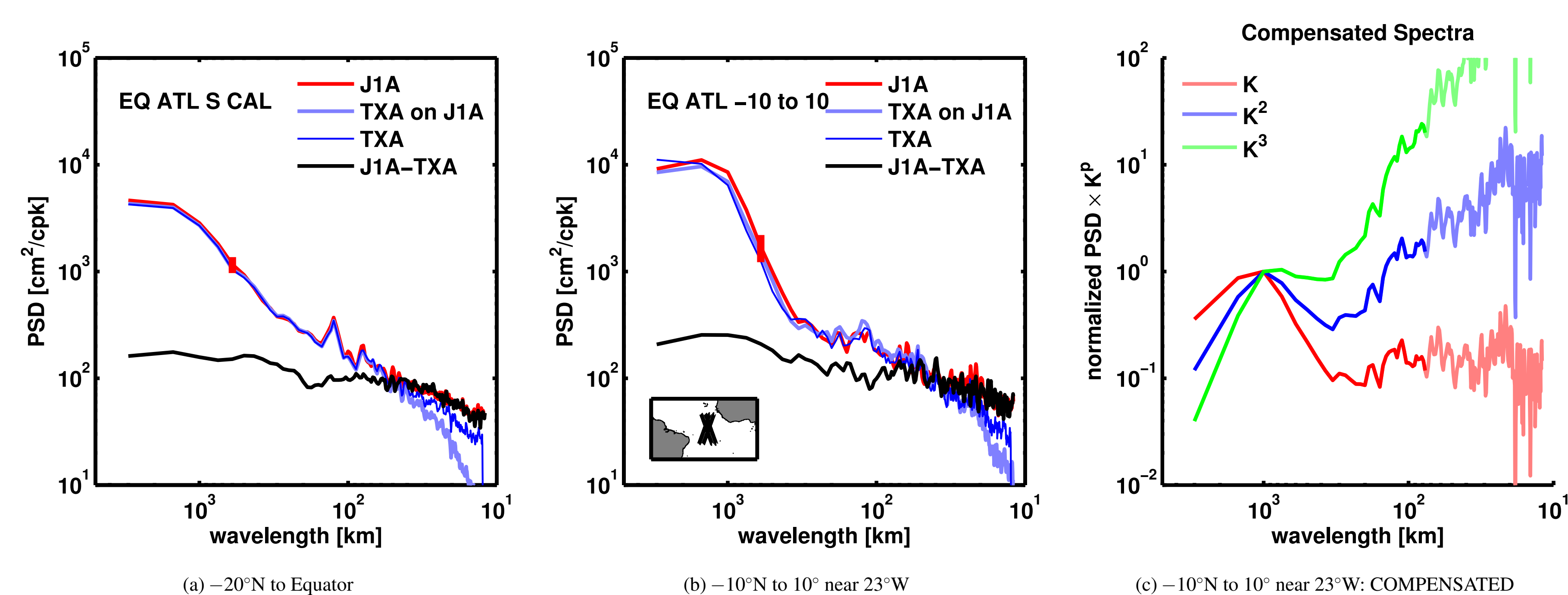
Figure 3: SSH spectra from 21 orbit cycles during the TOPEX/POSEIDON (TXB) – Jason-1 (J1A) calibration phase. (A) Spectra from −20°N to 0, same tracks as used in AX08 comparison, illustrates comparison of J1A and TXB. The spectra diverge at about 70km wavelength. In order to compute the spectrum of SSH differences it is necessary to interpolate from one satellite's ground track to the other; this reddens the interpolated SSH spectrum, and biases low the estimated altimeter noise at scales less than 80km. (B) Spectra from ground tracks centered at the equator are lower energy from those nearby. (C) The compensated spectra show that the mesoscale spectral slope is uncertain at wavelengths shorter than 200km due to a possible tidal peak and proximity to the noise level. Gray shading indicates where the signal-to-noise ratio of the noise-corrected spectrum is less than 2.

In Situ Current Measurements from the PIRATA Mooring at 23°W on the Equator

(a) AX08 average transect.

(b) ADCP mean and first 3 vertical modes.

(c) Frequency spectrum at 110m
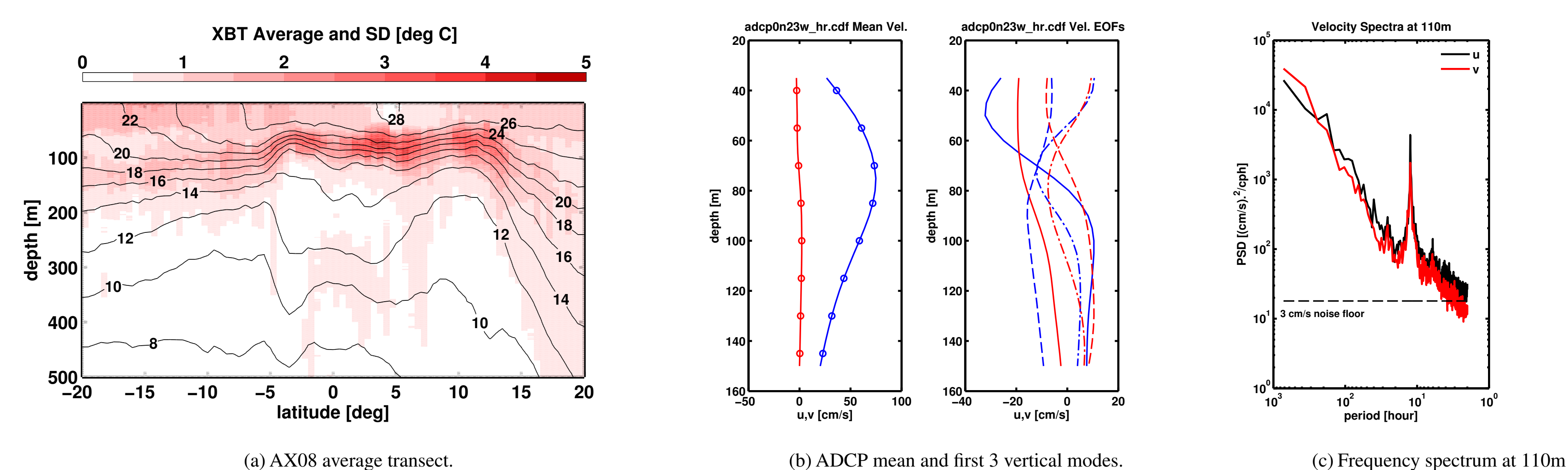
Figure 4: In situ current observations were measured hourly by ADCP on a PIRATA mooring from 2008 to 2010. Although regridded to 5m intervals, the nominal vertical resolution of the currents is 9m. (A) Mean and standard deviation of the temperature field from the nearby AX08 transects provides context. Most variability is associated with the near-surface thermocline. (B) The mean and first three vertical modes account for more than 90% of the variance in the currents. (C) The power spectrum of the currents at 110m, below the surface mixed layer, shows a large peak near 12hr. Note also that the spectrum appears to shift on either side of the tidal band. The anisotropy $S_{uu}(\omega)/S_{vv}(\omega) \approx 1.5$ is nearly constant across this shift and for all periods shorter than 100hr.

(a) Compensated and de-tided spectra.

(b) Complex demodulation centered at M2.

(c) Spectra of demodulated amplitude and phase.
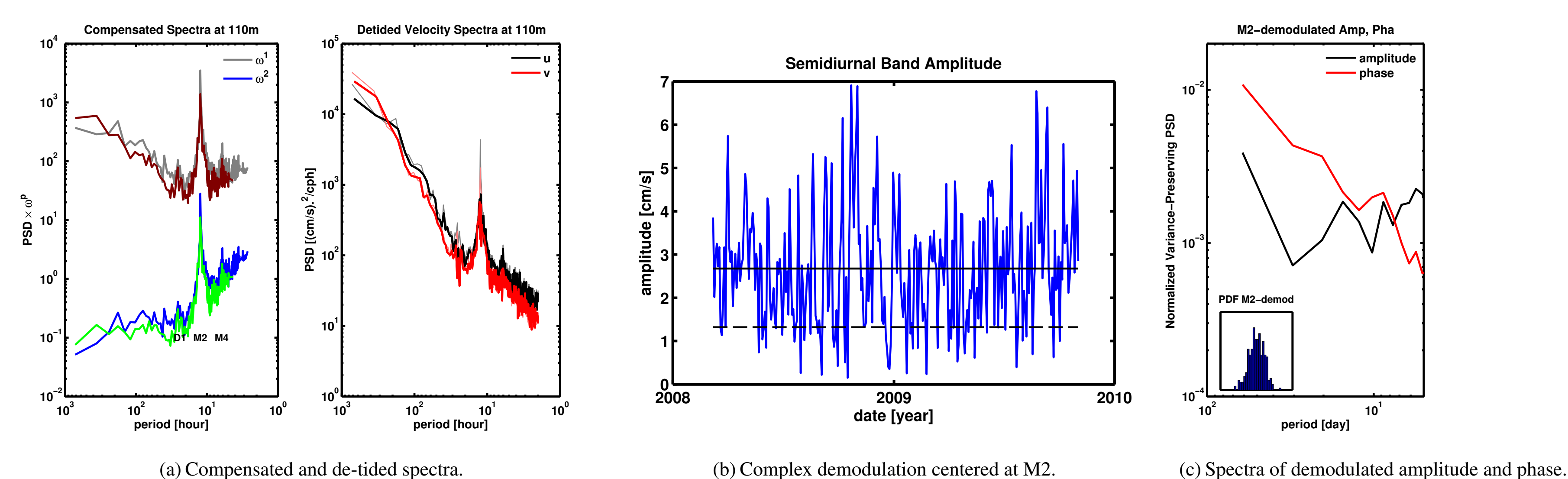
Figure 5: (A) The compensated spectrum (left) shows that subtidal currents folllow ω^{-2} scaling. The spectral range is not adequate to distinguish ω^{-2} and $\omega^{-5/3}$ scaling. The spectral slope changes across the tidal peak, but the slope of the high-frequency range is uncertain. Diurnal (D1), semi-diurnal (M2), and quarter-diurnal (M4) peaks are indicated. (B) The amplitude of the semi-diurnal tide determined by diurnal, semidiurnal, and quarter-diurnal tidal fits over a 2-day window is shown. It is highly variable and shows no sign of spring-neap variability. Solid black line is the average semi-diurnal amplitude; dashed line is the phase coherent M2 tidal amplitude determined from the entire record. (C) Variance-preserving power spectra of the semi-diurnal demodulate amplitude and phase show the broadband nature of the variability; the phase spectrum is red. Inset shows the in-phase component of the semi-diurnal demodulate; it is close to Gaussian.

2011 OSTST
San Diego, CA
October 19-21, 2011

Edward D. Zaron
Department of Civil and Environmental Engineering
Portland State University
zaron@cee.pdx.edu